THE PENNSYLVANIA STATE UNIVERSITY
SCHREYER HONORS COLLEGE

DEPARTMENT OF AEROSPACE ENGINEERING

CALIBRATION OF INFRARED WINDOW AND STUDY OF THE WIND TUNNEL PROPERTIES

CHRISTOPHER J. AXTEN
SPRING 2016

A thesis
submitted in partial fulfillment
of the requirements
for a baccalaureate degree
in Aerospace Engineering
with honors in Aerospace Engineering

Reviewed and approved* by the following:

Cengiz Camci
Professor of Aerospace Engineering
Thesis Supervisor

Mark Maughmer
Professor of Aerospace Engineering
Faculty Reader

George A. Lesieutre
Professor of Aerospace Engineering
Head of the Department of Aerospace Engineering

* Signatures are on file in the Schreyer Honors College.

ABSTRACT

In the world of turbomachinery, increasing the efficiency of the air-breathing gas turbine engine is always the end goal, which is accomplished by operating at the highest possible turbine inlet temperature. However, this leads to issues in designing turbine blades, typically made of nickel alloys, that are capable of withstanding the thermal stresses associated with combustor exit temperature. Thus, bled off air is commonly passed through turbine blades in a serpentine pattern and over pin fins within the blades to increase the blade cooling. The most common pin fin design uses a circular cross section, however past studies have shown other cross sections are more favorable. Different pin fin geometries, and configurations of pin fins, produce varying temperature fields around the pin fins, and thus can produce different convective heat transfer results. An optimized pin fin design and configuration would improve the convective heat transfer while not compromising on the pressure losses over the pin fins, which would ultimately result in turbine blades reaching higher temperatures and thus higher efficiencies. Past studies have performed their measurements with liquid crystal thermography on the endwall to determine the convective heat transfer coefficients. This study seeks to instead use infrared thermography to measure the temperature field of the endwall to determine the convective heat transfer characteristics. This method requires calibrating an infrared window that is set to view the heated endwall, which acts as the test section. The experiments were conducted using a FLIR T620 high resolution infrared imaging camera. The test section of the wind tunnel was set up with an infrared window from Edmund Optics. One endwall of the test section is uniformly heated by supplying different voltages, from 0 to 75 Volts, to a thermofoil Minco heating element for various velocities, ranging from 20 meters per second to 30 meters per second. The transmission losses, conduction

losses, and convective heat transfer coefficient were determined from infrared images and thermocouple temperature readings. The flow around through the tunnel was observed and through the recorded temperature field the convective heat transfer coefficient of the test section was calculated. The entire experiment was conducted in the Turbomachinery Heat Transfer Lab open loop wind tunnel.

TABLE OF CONTENTS

LIST OF FIGURES iii

LIST OF TABLES iv

LIST OF EQUATIONS v

ACKNOWLEDGEMENTS vi

Chapter 1 INTRODUCTION 1

APPLICATIONS OF INFRARED IMAGERY FOR GAS TURBINE COOLING 1
PREVIOUS STUDIES ON PIN FIN GEOMETRIES 2

Chapter 2 EXPERIMENTAL METHOD 3

WIND TUNNEL PROPERTIES 4
PRESSURE TRANSDUCER CALIBRATION 5
WIND TUNNEL MEASUREMENTS 6
INFRARED WINDOW MEASUREMENT METHOD 8

Chapter 3 EXPERIMENTAL RESULTS AND DISCUSSION 10

INFRARED WINDOW CALIBRATION 10
INFRARED IMAGE QUALITY 13

Chapter 4 UNCERTAINTY ANALYSIS 15

UNCERTAINTY CALCULATIONS 15
DISCUSSION OF UNCERTAINTY 17

Chapter 5 CONCLUSIONS AND FUTURE WORK 19

Appendix ADDITIONAL UNCERTAINTY EQUATIONS AND CODE 20

BIBLIOGRAPHY 23

LIST OF FIGURES

Figure 1: Wind Tunnel Setup for Experiment 3

Figure 2: Calibration of Transducer A 5

Figure 3: Calibration of Transducer B 6

Figure 4: Distance vs Velocity - Wind Tunnel 7

Figure 5: Velocity vs Pressure - Wind Tunnel 7

Figure 6: Velocity vs Frequency - Wind Tunnel 8

Figure 7: Infrared Camera Zoomed in the Thermocouple 9

Figure 8: Voltage vs. Temperature - 20m/s 12

Figure 9: Voltage vs. Temperature - 30m/s 12

Figure 10: Local Convective Heat Transfer at Thermocouple Location 13

Figure 11: Box Over Thermocouple 14

Figure 12: Local Convective Heat Transfer Coefficients in Box 14

Figure 13: Uncertainty Percentage vs Voltage 18

LIST OF TABLES

Table 1: Uncertainty Differential Values.....17

LIST OF EQUATIONS

Equation 1: Conservation of Energy for Radiation.....1

Equation 2: Total Heat Flux Equation 15

Equation 3: Convective Heat Flux Equation.....15

Equation 4: Conductive Heat Flux Equation 15

Equation 5: Convective Heat Transfer Coefficient.....16

Equation 6: Differential of the Convective Heat Transfer Coefficient 16

Equation 7: Current Uncertainty Differential 20

Equation 8: Resistance Uncertainty Differential.....20

Equation 9: Heater Area Uncertainty Differential 20

Equation 10: Conduction Loss Uncertainty Differential 20

Equation 11: Infrared Camera Temperature Uncertainty Differential.....21

Equation 12: Adiabatic Wall Temperature Uncertainty Differential.....21

Equation 13: Experimental Uncertainty.....21

ACKNOWLEDGEMENTS

Over the course of my time at Penn State, many people have encouraged and positively influenced me in a permanent way. First, I must thank Dr. Cengiz Camci for advising me over the course of my thesis work, along with his providing insight and encouragement when things did not go right the first time. I must also thank Dr. Phillip Morris, for his time and advice as my honors advisor, and Dr. Mark Maughmer, for his constant guidance and challenging me through the sailplane class.

I do not know how I would have managed without my fellow researcher Sowmya Raghu, who always planned ahead and worked endlessly to ensure our research was of the highest quality. I must also thank Jason Town for taking the time to teach me the basics of turbomachinery and advising me during the beginning of my research.

My friends and family have been a large part of my support as well. My friend and roommate Daniel Schultz has always provided an ear to listen to the hardships of aerospace engineering. I must acknowledge Matthew Shaw for sharing my pain every step of the way. Thanks to my friends for the support and the comic relief they provide: Isaac Kim, Justin Kibler, Van Rude, and all of those who I cannot name. I must thank my parents, Victor and Carol, and my stepmom Nancy for their constant encouragement and support, along with all of my brothers and sisters. Lastly, I must acknowledge the Dunkin' Donuts on College Avenue, across from the Hammond Building, for supplying my continual need for caffeine.

Chapter 1

INTRODUCTION

The infrared spectrum was discovered by Sir William Herschel in 1800 and a short time later infrared light began use as a means of thermal measurement. The concept is based on radiation heat transfer which occurs through electromagnetic waves. When the electromagnetic waves come into contact with a body parts of the energy are absorbed, reflected, or pass through the body, with the fraction of each being denoted by α_r, ρ_r, and τ_r and referred to as absorptivity, reflectivity, and transmissivity respectfully [1]. Since energy is always conserved the absorptivity, reflectivity, and transmissivity of the interaction of an electromagnetic wave with a body must be:

$$\alpha_r + \rho_r + \tau_r = 1$$

Equation 1: Conservation of Energy for Radiation

These coefficients vary depending on the wavelength of the radiation and the properties of the body with which the electromagnetic wave is interacting. Ultimately, using the radiation emitted by a body, especially radiation emitted in the infrared wavelength spectrum, its temperature can be determined using several laws of radiation. Thus, infrared cameras discern the temperature of a body using the radiation it emits in the infrared spectrum.

APPLICATIONS OF INFRARED IMAGERY FOR GAS TURBINE COOLING

Within academia infrared imagery has been used for a number of different studies. One particular study by Dr. Giovanni Carlomagno used infrared imagery to analyze transient natural

convection, impinging jets, airfoil transition/separation, rotating surfaces, 180°-turn channels and ribs, and hypersonic flows [2]. The study did not necessarily produce any information that is not already known, however it proved the feasibility of using infrared imagery to analyze the heat transfer properties under very different conditions. Many of these experiments were especially applicable to gas turbine research, such as the rotating surfaces and 180°-turn channels and ribs, since these are applications characteristically found in turbines. The article also made the points that infrared imagery non-intrusively measures the flow and records a 2D field of data. Both of these points offer arguments to the position of using infrared imagery over thermocouples in many heat transfer experiments.

PREVIOUS STUDIES ON PIN FIN GEOMETRIES

Studies have also been conducted on analyzing different pin fin geometries, with the intent of determining an optimum design for convective heat transfer while minimizing pressure losses. One such study was done by Oğuz Uzol for a dissertation work at the Pennsylvania State University. Pin fins with the following geometries: Circular as a baseline, oscillating, elliptical with a major axis 1.67 times the minor axis, and elliptical based on the NACA 0024, were all analyzed for their convective heat transfer and aerodynamic characteristics. Liquid crystal thermography was used to determine the endwall convective heat transfer properties, and wake total pressure surveys and wake flow field measurements were used to determine the aerodynamic properties of each geometry. The study concluded with identifying the oscillator fin as performing worse than the circular pin fin in heat transfer, but better than the circular fin minimizing pressure losses. Similarly, both elliptical fins produced about 25% less heat transfer

levels than the circular fin, however the total pressure reduction was on the order of 100% to 200% [3]. Implementing infrared imagery on a similar study would produce higher resolution temperature field measurements and enable the researcher to more accurately determine the convective heat transfer characteristics of each design.

Chapter 2

EXPERIMENTAL METHOD

The wind tunnel was originally in sections so it was assembled prior to any experimentation. This required the wind tunnel to be recalibrated as any past properties of the tunnel may have been changed due to a slight alignment differences, gaps, compressor performance, etc. Once the tunnel properties were determined the infrared window and endwall emissivity values were determined.

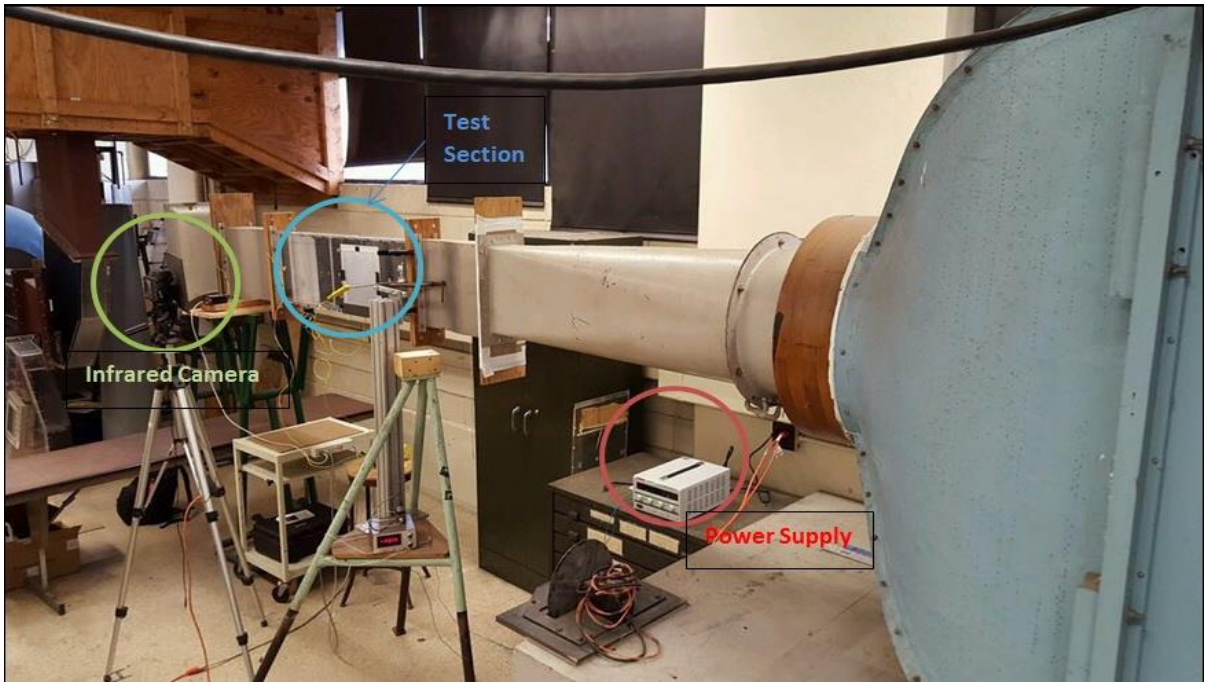


Figure 1: Wind Tunnel Setup for Experiment

WIND TUNNEL PROPERTIES

The wind tunnel in consideration is an open circuit wind tunnel. The various parts of the tunnel are as follows

- An axial air blower
- A plenum chamber
- A circular nozzle with high area ratio
- A circular to rectangular transition duct
- A converging section
- The test section with infrared window
- A diverging nozzle
- A diffuser (discharges air to the ambient conditions)

Each section was bolted together with silicon between them and as flush as possible to minimize the effects on the boundary layer when the flow travels between tunnel sections. Additionally, screens were placed at each end of the plenum chamber to produce a uniform flow after the compressor.

The infrared window was 30.5cm X 30.5cm square, stock number 32-809 from Edmund Optics, and the test section walls were made of clear acrylic plexi glass of 1.2cm thickness. The Minco thermofoil heater had a dimension of 25cm X 37.5 cm, model number 5185 with 17.6Ω of resistance, and was supplied with voltages ranging from 55V – 75V by using the DC power supply, which provided up to 110V and 10A current. There was a 2mm Depron sheet present in the end wall to minimize conductive losses and the Depron and heater filament were painted black to minimize radiative losses.

Three thermocouples were installed: one in the test section, exposed to the flow, for calibrating the infrared camera's emissivity and other properties, another outside of the tunnel to determine the conduction losses through the wall, and the last one to measure the ambient temperature near the test section.

PRESSURE TRANSDUCER CALIBRATION

The pressure transducers were calibrated with the slant tube manometer; the calibration graphs are present below.

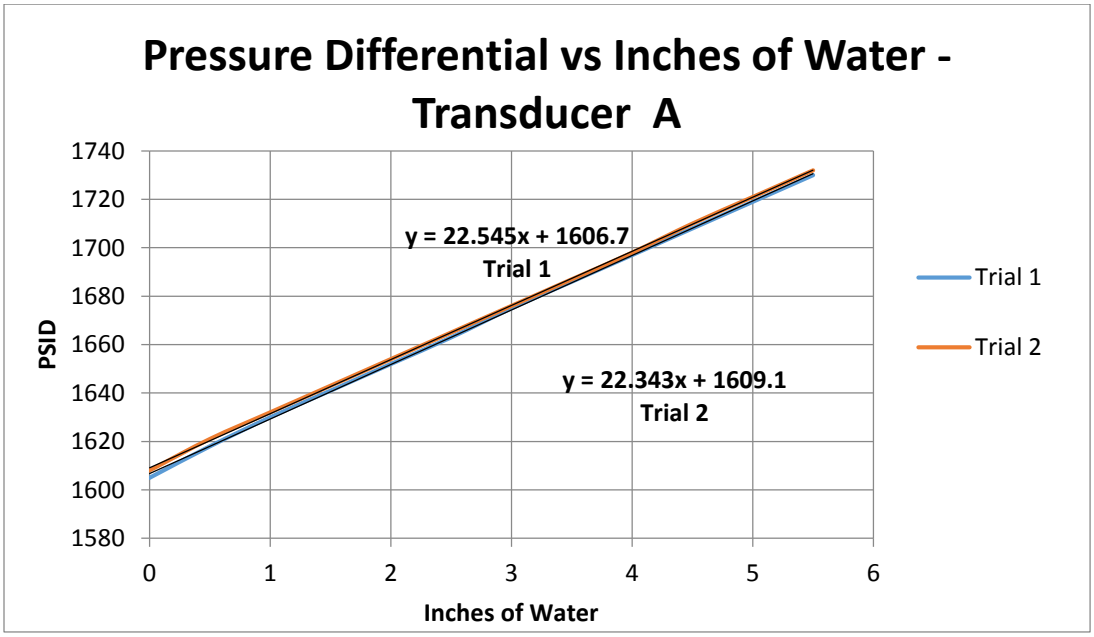


Figure 2: Calibration of Transducer A

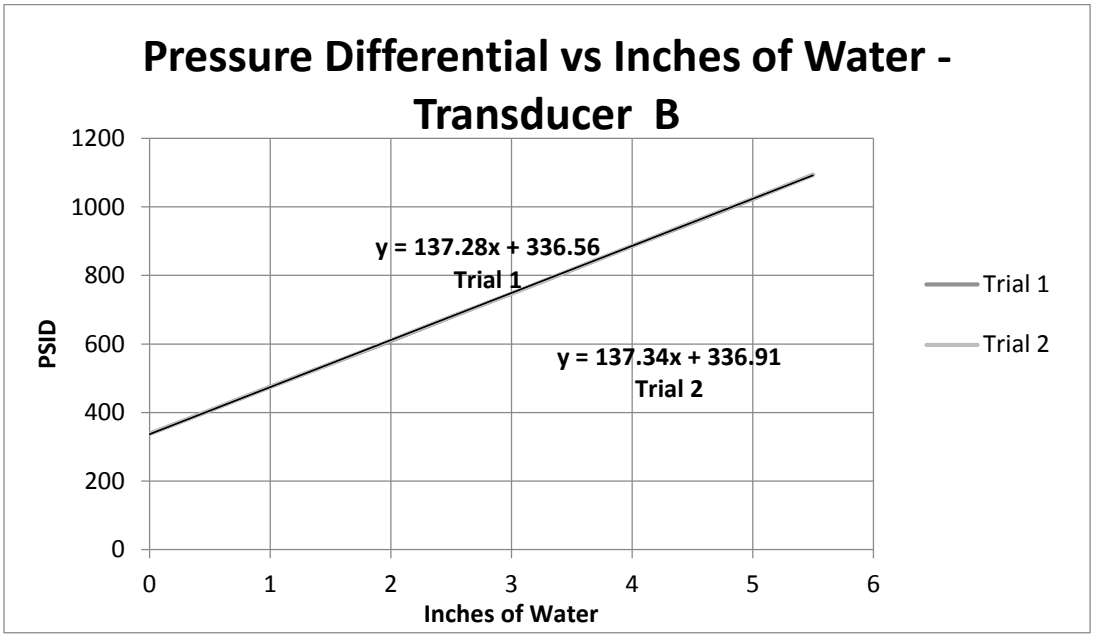


Figure 3: Calibration of Transducer B

WIND TUNNEL MEASUREMENTS

The calibrated pressure transducer was then used with a pitot static probe to determine the velocity profile, velocity and pressure relationship, and the relationship between the compressor fan speed and the velocity of the tunnel. The velocity profile of the tunnel showed to be primarily uniform away from the boundary layer of the wall, which verified the tunnel was experiencing no flow disturbances from gaps or misalignments between the sections.

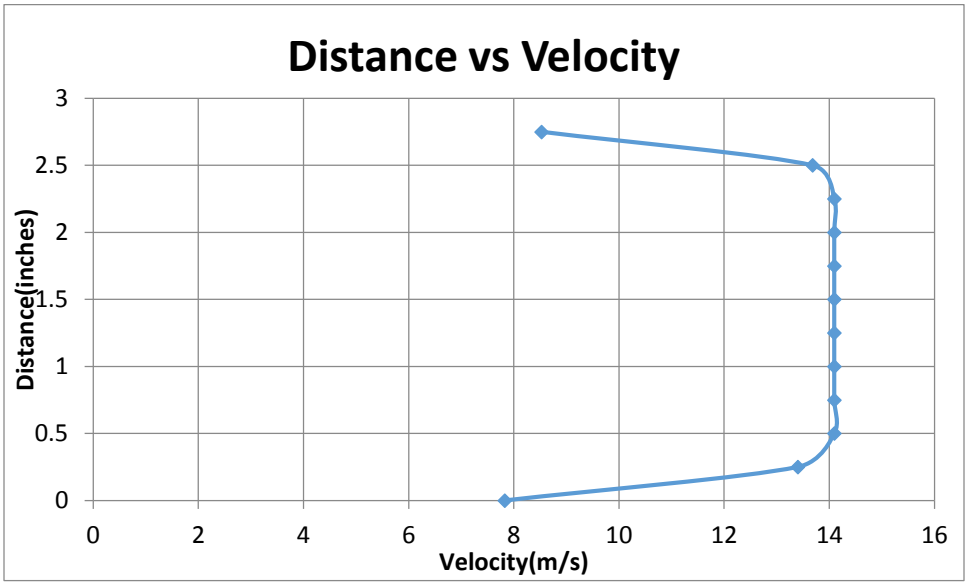


Figure 4: Distance vs Velocity - Wind Tunnel

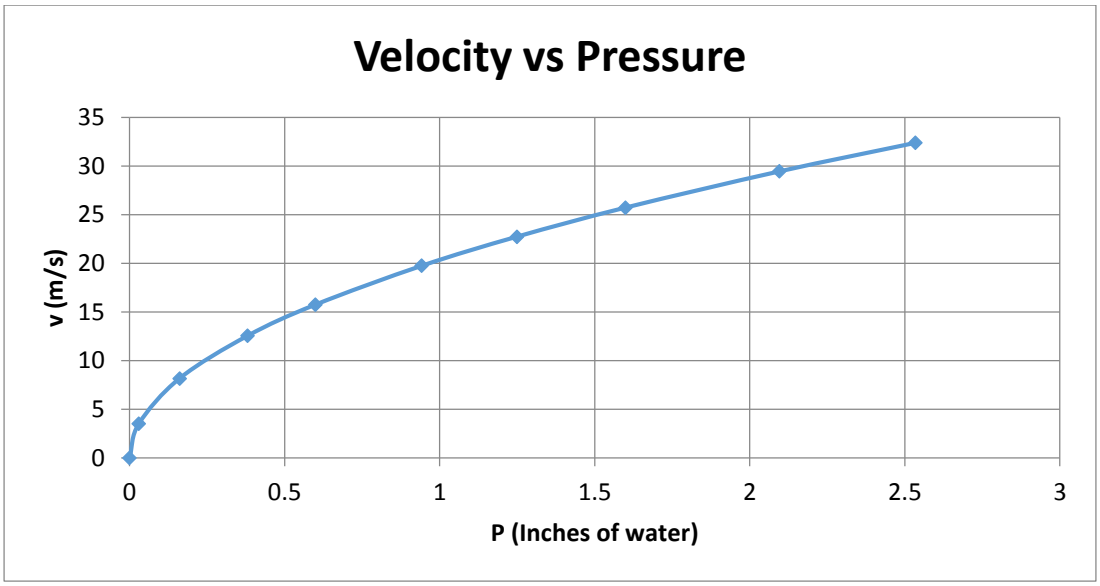


Figure 5: Velocity vs Pressure - Wind Tunnel

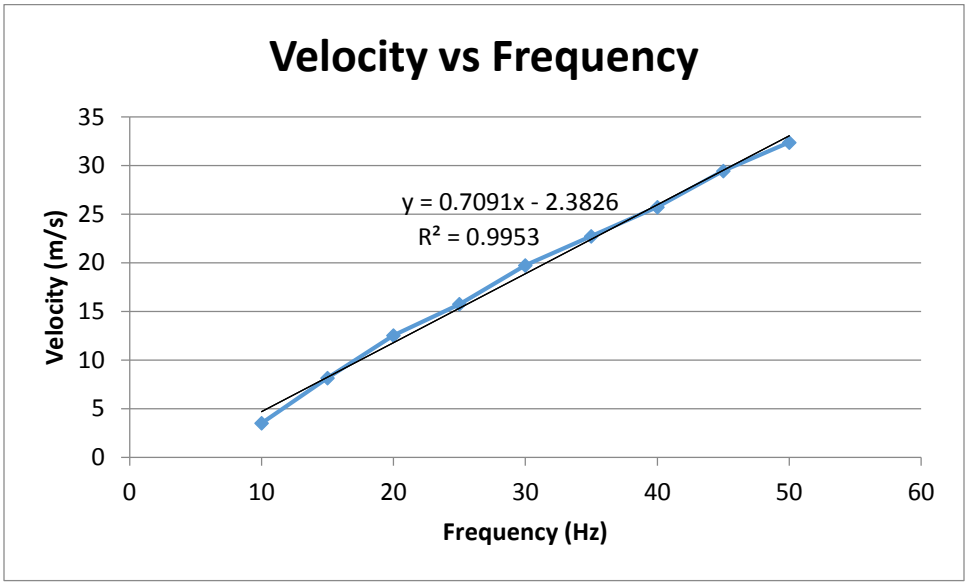


Figure 6: Velocity vs Frequency - Wind Tunnel

INFRARED WINDOW MEASUREMENT METHOD

The infrared camera had a measurement resolution of 640x480 pixels and was placed at a location of 1 meter from the test section to capture the field of view of the infrared window. The infrared camera was typically used with a Spot reading and Box reading (0.25 in X 0.25in area). The Box value was an average of the temperatures over the surface but FLIR's software provides the ability to know the temperature of each pixel within the Box, and thus find line averages and gradients. Additionally, the FLIR software package allows the user to draw additional spots, boxes, circles, etc. after the image was taken so the user is not constrained to the readings taken during the picture. The figure below shows the user interface of the camera.

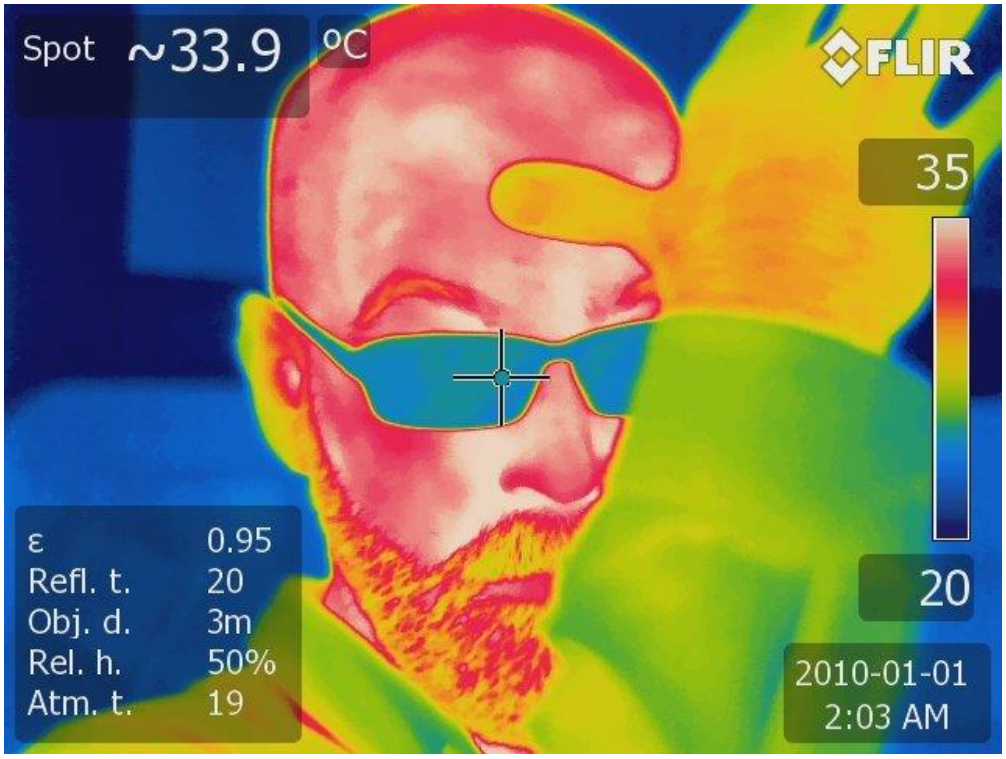


Figure 7: Infrared Camera User Interface

Initially, the infrared window was reflecting infrared radiation originating from outside of the test section, such as from the user or itself, which was causing the infrared camera to record values that were false. This was addressed by fitting a piece of black Depron foam over the lenses so the bulk of the camera cannot be seen from the front. This can be seen in Figure 1: Wind Tunnel Setup for Experiment.

Chapter 3

EXPERIMENTAL RESULTS AND DISCUSSION

INFRARED WINDOW CALIBRATION

In order for the infrared camera to be used to obtain an accurate convective heat transfer profile it had to be properly calibrated with the infrared window being used. The calibration of the infrared camera was done with the camera setup 1m distance from the test section. For the first set of experiments a set of 9 points were marked out on the ground in front of the test section to determine if viewing the test section, without the infrared window in place, at various angles effected the readings. The center point was from which the camera was first set and the other points were marked 2 inches to the left, 2 inches up and 2 inches left, 2 inches up, etc. around the center point thereby producing a square around the center point. This setup provided a 3X3 matrix with the set of values of the temperature readings from the thermocouple, the Spot (set on the tip of the Thermocouple), and the Box (centered on the thermocouple) to compare. The experiments ultimately showed that viewing the test section at various angles did not have effect on the infrared camera's readings. This initial calibration was done with a DC power supply over a range of voltages from 0V – 20V, which was eventually increased to 0V – 70V, however since the placement had no effect on the results it was assumed to have no effect on the camera throughout the later operating range as well.

Running from 10V to 70V for 5 minutes at every tenth voltage provided a relationship between the reading of the infrared camera and thermocouple in the test section with the infrared window in place. This calibration was first done with no flow in the tunnel by matching the value of the infrared camera to the value of the thermocouple as closely as possible, without the

infrared window, using only the emissivity value built into the camera to determine the emissivity of the endwall with the heater (painted black surface). Next, the window was replaced and the same experiment was run with no flow to match the camera with the transmissivity of the infrared window. The emissivity was determined to be 0.97 for the endwall and the transmission characteristic of the infrared camera to be used for the used infrared window was found to be 75%**.** Using these properties, the infrared camera and thermocouple agreed over the range of voltages used.

These calibration properties were then used with a flow running through the tunnel, however the readings of the thermocouple and infrared camera did not match for either of the experiments with a flow running through the tunnel. Although, it can be noted that the curves for the thermocouple and infrared camera for both tunnel velocities are almost perfectly parallel. This is believed to have happened because the thermocouple in the test section was covered with a thick piece of tape when it was installed. Therefore, when there was not a flow in the tunnel, and thus no convective heat transfer, the tape had a negligible effect on the temperature difference between the thermocouple and the infrared camera. When the flow was introduced the thickness of the tape allowed the thermocouple to maintain a different temperature than the endwall temperature that the infrared camera was viewing. Even though the surface mounted thermocouple did not provide the true temperature of the fluid-solid interface, it was useful in determining the infrared transmission loss through the infrared window.

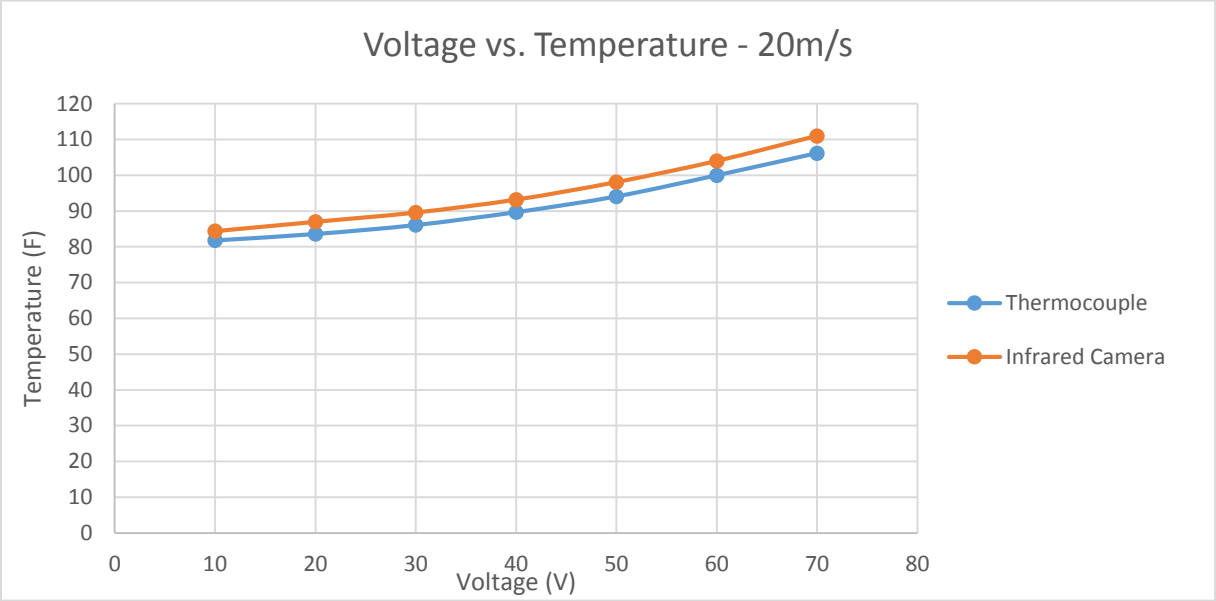


Figure 8: Voltage vs. Temperature - 20m/s

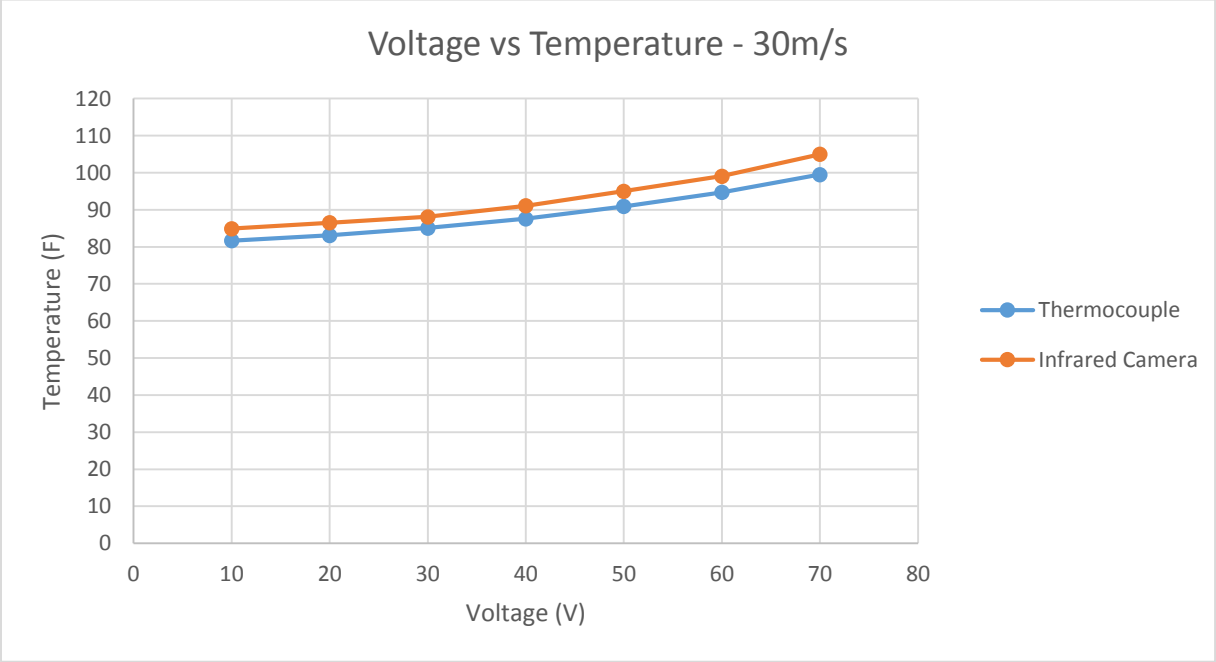


Figure 9: Voltage vs. Temperature - 30m/s

INFRARED IMAGE QUALITY

Using infrared imaging produced high resolution images of the temperature field. The infrared camera utilized for this study produced a 640 x 480 image, which generated an approximately 460 x 350 image of the test section when the camera was mounted 1 meter from the wind tunnel. This translates to determining the local convective heat transfer coefficient at over 161,000 points in the test section, which can provide a very detailed analysis of the heat transfer characteristics of the test section. The values in the plot below were determined using the infrared camera at the location of the thermocouple.

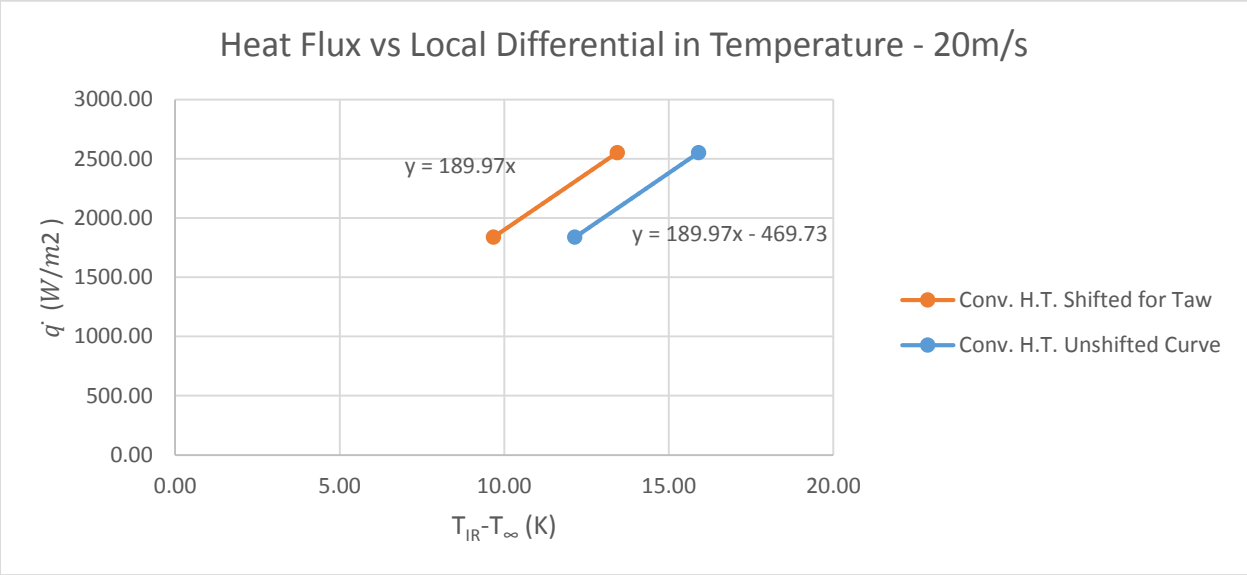


Figure 10: Local Convective Heat Transfer at Thermocouple Location

The following image was taken at 55V with a 30m/s flow. In Figure 12: Local Convective Heat Transfer Coefficients in Box (Over the Thermocouple) the box is analyzed to determine the convective heat transfer coefficient over the region where the thermocouple was mounted and covered with a piece of tape. The small region being analyzed produced a somewhat grainy image of the convective heat transfer coefficient over the surface, although larger images produce a very high resolution analysis of the surface.

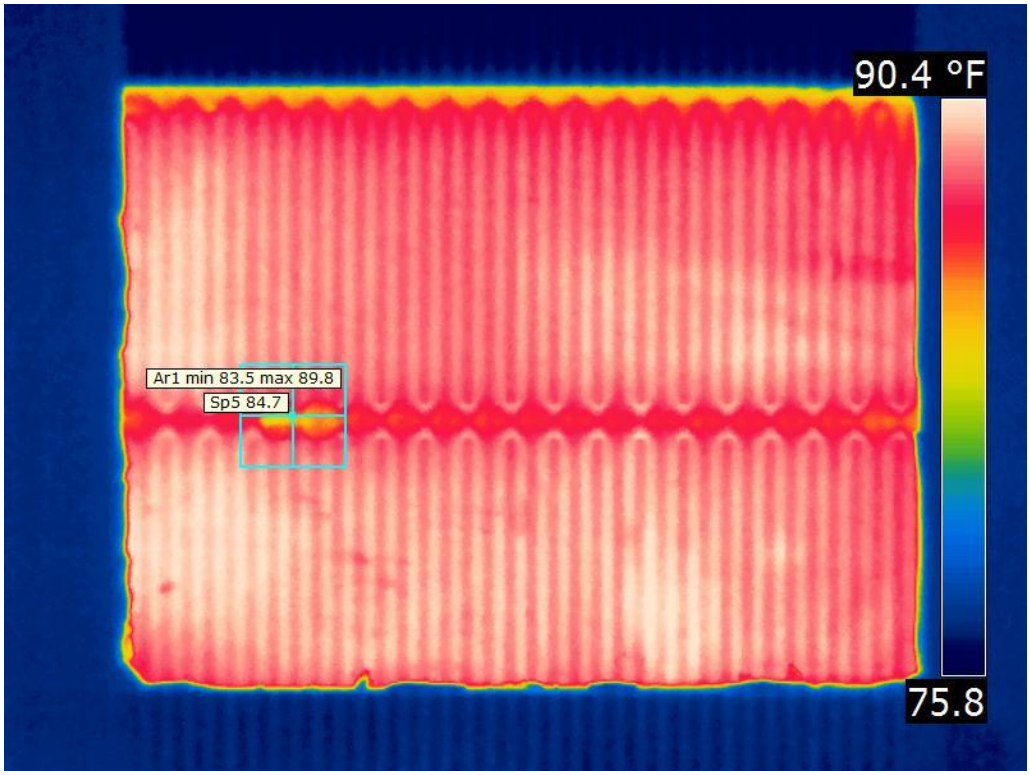


Figure 11: Box Over Thermocouple at 55V in 30 m/s Flow

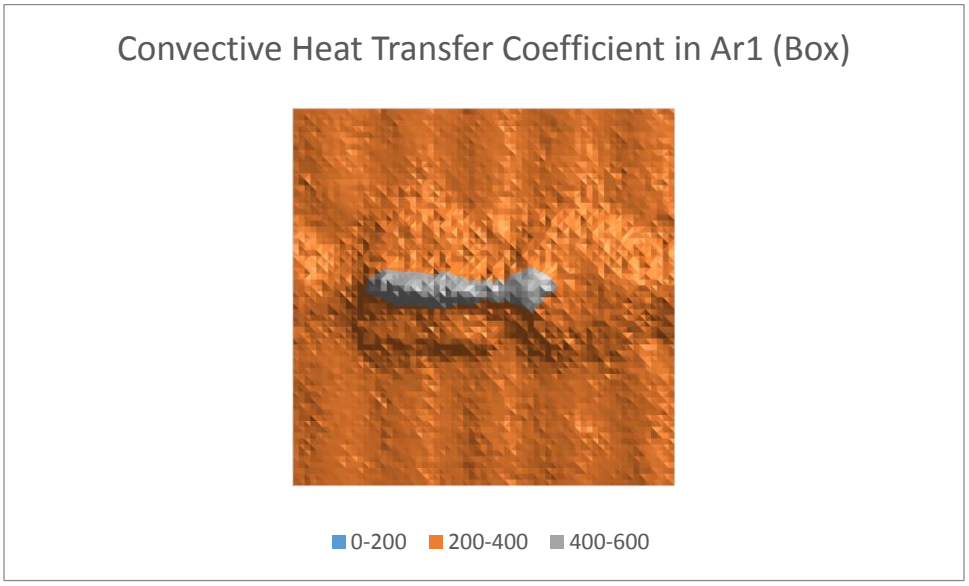


Figure 12: Local Convective Heat Transfer Coefficients in Box (Over the Thermocouple)

In summary, the infrared camera used for the experiment produces a high resolution picture and has an abundance of potential in determining the convective heat transfer characteristics of a flow.

Chapter 4

UNCERTAINTY ANALYSIS

Due to imperfections in the equipment and analysis, a level of experimental uncertainty must be put forward to address any discrepancies between the achieved results and the results of computational analysis, theoretical analysis, etc.

UNCERTAINTY CALCULATIONS

Determining the convective heat transfer coefficient, h_{conv}, was the ultimate objective of the study, therefore the uncertainty analysis was based upon h_{conv}. The process for determining the uncertainty of the convective heat transfer coefficient is listed below:

$$\frac{V^2}{RA_h} = \dot{q}_{total} = \dot{q}_{conv} + \dot{q}_{cond}$$

Equation 2: Total Heat Flux Equation

Where $\dot{q}_{conv}$ is defined as:

$$\dot{q}_{conv} = h_{conv} * (T_{IR} - T_{aw})$$

Equation 3: Convective Heat Flux Equation

And $\dot{q}_{cond}$ is defined as:

$$\dot{q}_{cond} = k_{wall} * \frac{T_{C1} - T_{C2}}{t_{wall}}$$

Equation 4: Conductive Heat Flux Equation

Which can be rewritten as:

$$h_{conv} = \frac{\frac{V^2}{RA_h} - \dot{q}_{cond}}{T_{IR} - T_{aw}}$$

Equation 5: Convective Heat Transfer Coefficient

The adiabatic wall temperature, T_{aw}, is the theoretical wall temperature achieved when the heat flux through the wall is zero, meaning it is thermally insulated. This provides a consistent metric for which to calculate the convective heat transfer coefficient. Using the definition of the convective heat transfer coefficient in Equation 5: Convective Heat Transfer Coefficient, the differential value of h_{conv} is calculated as follows:

$$\delta h_{conv} = \sqrt{\begin{matrix}\left(\frac{\partial h}{\partial V} * \delta V\right)^2 + \left(\frac{\partial h}{\partial R} * \delta R\right)^2 + \left(\frac{\partial h}{\partial A_h} * \delta A_h\right)^2 + \left(\frac{\partial h}{\partial \dot{q}_{cond}} * \delta \dot{q}_{cond}\right)^2 \\ + \left(\frac{\partial h}{\partial T_{IR}} * \delta T_{IR}\right)^2 + \left(\frac{\partial h}{\partial T_{aw}} * \delta T_{aw}\right)^2\end{matrix}}$$

Equation 6: Differential of the Convective Heat Transfer Coefficient

The differentials of each the terms involved in the calculation of convective heat transfer coefficient can be found in the Appendix

ADDITIONAL UNCERTAINTY . The differential values used to determine the terms A through F come from the uncertainty associated with the measurement devices used and are listed below during baseline conditions when the velocity in the tunnel is 20m/s.

Terms of Uncertainty	Assigned Variable	Baseline Experiment Value	Estimated Differential Measurement Value
Voltage	V	$65.0V$	$\pm 0.1V$
Resistance	R	17.6Ω	$\pm 0.1\Omega$
Heater Area	A_h	$0.09375m^2$	$\pm 1 * 10^{-6}m^2$
Conduction Heat Flux	$\dot{q}_{cond}$	$8.3\frac{W}{m^2}$	$\pm 0.1\frac{W}{m^2}$
Infrared Temperature	T_{IR}	$317.4K$	$\pm 0.2K$
Adiabatic Wall Temperature	T_{aw}	$304.0K$	$\pm 0.2K$

Table 1: Uncertainty Differential Values

Performing the calculations with above numbers, the baseline experiment has an uncertainty of 1.71%.

DISCUSSION OF UNCERTAINTY

Using the differential values in Table 1, the uncertainty percentage for various voltages and tunnel velocities could be computed to determine the uncertainty percentage at during various experiments.

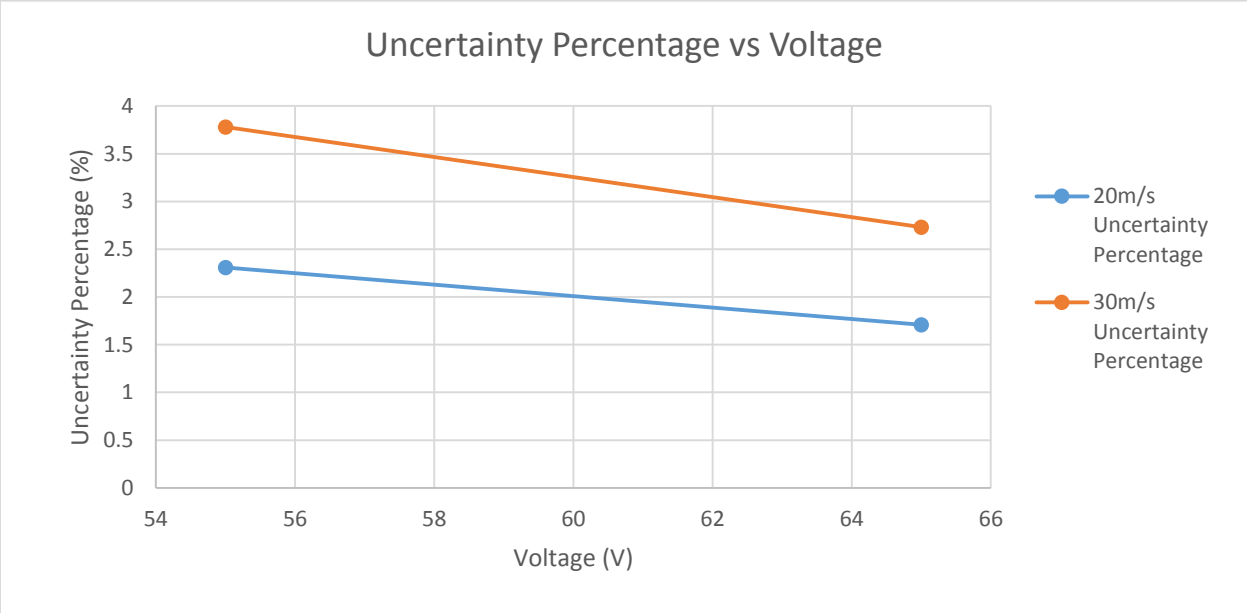


Figure 13: Uncertainty Percentage vs Voltage

Being that the calculated uncertainty values are below 5%, it is safe to assume that the experimental data is within a tolerable range of uncertainty. It can be noted that the uncertainty decreases with an increase in voltage, however it does not decrease by a very large amount. The uncertainty also seems to decrease with a lower tunnel velocity, as seen with the two velocities shown above.

An uncertainty analysis is a mathematical approximation of the uncertainty associated with an experiment, thus it is not perfect and does not take into consideration external factors beyond the capabilities of the measuring devices, such as human error. The uncertainty percentages obtained through this analysis seem very optimistic for what would be expected, a more realistic and probable uncertainty percentage is between 5% and 8%.

Chapter 5

CONCLUSIONS AND FUTURE WORK

Infrared imaging proved to be an effective method of analyzing the temperature field of the heated endwall of a wind tunnel while a flow is passing over the surface. This is substantial as it allows the local convective heat transfer coefficient to be determined over the entire surface, opposed to at a single location with a thermocouple, while being non-intrusive and producing accurate results. This concept has implications for future turbine blade cooling research, where improving the cooling process effectively leads to improved efficiency, which is ultimately the end goal.

Future research recommendations include introducing various geometries into the flow and using the temperature field produced by an infrared camera to determine the local and average convective heat transfer coefficients. This will allow different shapes to be compared so that they may considered for turbine blade cooling design. Another recommendation for future work is introducing different configurations and combinations of the geometries into the flow to discover the how the interaction between the geometries effects their convective heat transfer capability, and optimize for a configuration that could be implemented in future gas turbine blades.

Appendix

ADDITIONAL UNCERTAINTY EQUATIONS AND CODE

$$A = \left(\frac{\partial h_{conv}}{\partial V} * \delta V\right)^2 = \left(\frac{2V\delta V}{RA_h(T_{IR} - T_{aw})}\right)^2$$

Equation 7: Current Uncertainty Differential

$$B = \left(\frac{\partial h_{conv}}{\partial R} * \delta R\right)^2 = \left(\frac{-V^2\delta R}{R^2A_h(T_{IR} - T_{aw})}\right)^2$$

Equation 8: Resistance Uncertainty Differential

$$C = \left(\frac{\partial h_{conv}}{\partial A_h} * \delta A_h\right)^2 = \left(-\frac{V^2\delta A_h}{{A_h}^2(T_{IR} - T_{aw})}\right)^2$$

Equation 9: Heater Area Uncertainty Differential

$$D = \left(\frac{\partial h_{conv}}{\partial \dot{q}_{loss}} * \delta \dot{q}_{loss}\right)^2 = \left(\frac{-\delta \dot{q}_{loss}}{T_{IR} - T_{aw}}\right)^2$$

Equation 10: Conduction Loss Uncertainty Differential

$$E = \left(\frac{\partial h_{conv}}{\partial T_{IR}} * \delta T_{IR}\right)^2 = \left(\left[-\frac{\frac{V^2}{RA_h} - \dot{q}_{loss}}{(T_{IR} - T_{aw})^2}\right] * \delta T_{IR}\right)^2$$

Equation 11: Infrared Camera Temperature Uncertainty Differential

$$F = \left(\frac{\partial h_{conv}}{\partial T_{aw}} * \delta T_{aw}\right)^2 = \left(\left[\frac{\frac{V^2}{RA_h} - \dot{q}_{loss}}{(T_{IR} - T_{aw})^2}\right] * \delta T_{aw}\right)^2$$

Equation 12: Adiabatic Wall Temperature Uncertainty Differential

$$Uncertainty\ \% = 100 * \left(\frac{dh_{conv}}{h_{conv}}\right) = 100 * \left(\frac{\sqrt{A + B + C + D + E + F}}{\frac{\frac{V^2}{RA_h} - \dot{q}_{loss}}{T_{IR} - T_{aw}}}\right)$$

Equation 13: Experimental Uncertainty

A MATLAB code was written to help perform the uncertainty calculation:

```
clc
clear
V = ;
R = 17.6;
Ah = 0.09375;
q_cond = ;
Tir = ;
Taw = ;
```

```
dV = 0.1;

dR = 0.1;

dAh = 0.000001;

dq_cond = 0.1;

dTir = 0.15;

dTaw = 0.15;


A = ((2*V*dV)/(R*Ah*(Tir-Taw)))^2

B = ((-V^2*dR)/(R^2*Ah*(Tir-Taw)))^2

C = ((-V^2*dAh)/(R*Ah^2*(Tir-Taw)))^2

D = ((-dq_cond)/(R*Ah*(Tir-Taw)))^2

E = (((-1*(((V^2)/(R*Ah))-q_cond))*dTir)/((Tir-Taw)^2))^2

F = ((((V^2)/(R*Ah)-q_cond))*dTaw/((Tir-Taw)^2))^2


UncertPercent = 100*(sqrt(A+B+C+D+E+F)/((((V^2)/(R*Ah))-q_cond)/(Tir-Taw)))
```

BIBLIOGRAPHY

[1] Meola C. and CARLOMAGNO G.M., "Recent Advances in the Use of Infrared Thermography," *Measurement Science and Technology*, Vol. 15, No. 1, Jul. 23, 2004, pp. 27-58.

[2] Carlomagno, G.M., "Some Thermographic Measurements in Complex Fluid Flows,". *Journal of Flow Visualization & Image Processing*, Vol. 17, No. 1, 2010, pp. 15-40.

[3] Uzol, O., "Novel Concepts and Geometries as Alternatives to Conventional Circular Pin Fins For Gas Turbine Blade Cooling Applications," Ph.D. Dissertation, Aerospace Engineering Dept., The Pennsylvania State University., University Park, PA, 2000.

[4] Özgür Gökçe, Z., "Endwall Shape Modification Using Vortex Generators and Fences to Improve Gas Turbine Cooling and Effectiveness," Ph.D. Dissertation, Aerospace Engineering Dept., The Pennsylvania State University., University Park, PA, 2012.

[5] "10 Things You Need To Know About Infrared Windows," IRISS, inc., URL: http://www.datacentir.com/downloads/files/10_Things_You_Need_to_Know_About_Infrared_Windows.pdf [cited 4 March 2016].

ACADEMIC VITA

Academic Vita of Christopher Axten
cjaxten@gmail.com

Thesis Title

Calibration of Infrared Window and Study of the Wind Tunnel Properities

Thesis Supervisor

Dr. Cengiz Camci

Education

Major: Bachelors of Science in Aerospace Engineering

Honors

Dean's List, all semesters
Sigma Gamma Tau member

Work Experience

Date: June 2015 – August 2015
Title: Engineering Student Trainee
Description: Accessed the fidelity of a mission level program and suggested improvements to the project sponsor
Institution/Company: Naval Air Systems Command - Patuxent River, MD
Supervisor's Name: Donald Booz

Date: August 2015 – Present
Title: Teaching Intern
Description: Ensure a safe lab space is maintained, participate in building a human powered airplane
Institution/Company: The Pennsylvania State University – State College, PA
Supervisor's Name: Dr. Mark Maughmer

Date: January 2016 – Present
Title: Teaching Intern
Description: Work as a mentor to the professor by lecturing, making assignments, and grading
Institution/Company: The Pennsylvania State University – State College, PA
Supervisor's Name: Steven Willits

Association Memberships/Activities

American Institute of Aeronautics and Astronautics, Student Member
Cru, Student Member